J Mater Sci (2007) 42:3190–3196
DOI 10.1007/s10853-006-1353-4

Synthesis of PANI/TiO_2–Fe^{3+} nanocomposite and its photocatalytic property

Jinzhang Gao · Shengying Li · Wu Yang · Gang Ni · Lili Bo

Received: 29 July 2005 / Accepted: 27 February 2006 / Published online: 15 January 2007

Abstract A convenient method for synthesizing highly photocatalytic activity PANI/TiO_2–Fe^{3+} nanocomposite was developed. The effect of calcination temperature on the phase composition of TiO_2 nanopowder was investigated. It was found that higher temperature could promote the formation of rutile phase. The nanocomposite was characterized by atomic force microscopy (AFM), transmission electron microscopy (TEM), infrared spectroscopy (IR) and X-ray diffraction (XRD). The results indicated that the nanohybrid was composed of TiO_2, Fe^{3+} and PANI. The photocatalytic property of the nanocomposite was evaluated by the degradation of methyl orange. In the presence of this catalyst, the degradation rate of methyl orange of 95.2% and 70.3% could be obtained under the UV and sunlight irradiation within 30 min, respectively. The apparent rate constant was 5.64×10^{-2} which is better than that of the Degussa P25.

Introduction

In 1972, Fujishima and Honda [1] discovered the photocatalytic decomposition of water on TiO_2 electrodes. This event marked the beginning of a new era in heterogeneous photocatalysis. Since then, TiO_2 has become a promising photocatalyst to remove environmental pollutants such as alcohols, phenols, aromatics, surfactants and dyes [2, 3]. Owing to the strongly oxidizability, nontoxicity and long-term photostability, nano-TiO_2 exhibits many advantages over the other photocatalysts, even bulk of TiO_2 [4]. However, there are still some drawbacks, such as the lack of a visible photoresponse, a low quantum yield and lower photocatalytic activity. In order to overcome these problems, some strategies have been investigated, including noble metal deposition, doping of metal or nonmetal ions, blending with another metal oxide, surface photosensitizing with dye and compositing with polymer [5]. Polyaniline (PANI) is one of the most familiar conducting polymers and shows many advantages in recombining nanomaterials compared with others. Moreover, the large internal interface area in PANI/inorganic nanocomposite enables an efficient separation of charge, which is very important for photovoltaic application [6]. Therefore, intense research interests have been focused on the PANI/inorganic nanocomposite [7]. PANI/TiO_2 nanocomposite combines the merits of PANI and nano-TiO_2 to develop the potential applications in many fields. Some studies on the optical and electronic properties of PANI/TiO_2 nanocomposite have been reported in recent years [8]. However, the information on the use of PANI/TiO_2 nanocomposite in photocatalytic system is rather scarce. In this paper, a highly photocatalytic activity PANI/TiO_2–Fe^{3+} nanocomposite is prepared via sol-gel and chemical oxidation methods, and characterized using the degradation of methyl orange as a probe reaction. The aim of this paper is to modify the property of TiO_2 by introducing of Fe dopant and PANI conducting polymer, and improving the photocatalytic activity of TiO_2.

J. Gao (✉) · S. Li · W. Yang · G. Ni · L. Bo
College of Chemistry and Chemical Engineering, Northwest Normal University, Lanzhou 730070, P.R. China
e-mail: jzgao@nwnu.edu.cn

Experimental

Synthesis of PANI/TiO_2–Fe^{3+} nanocomposite

TiO_2 nanopowder was synthesized from the tetrabutyl titanate ($Ti(OBu)_4$) by the sol-gel method. A 8.5 mL of $Ti(OBu)_4$ was dissolved in 34 mL of absolute ethanol with stirring for 5 min, then 2 mL of diethanolamine (DEA) was added to the above solution, stirring for additional 1 h to get the mixture solution A. Another mixture solution B containing 5 mL absolute ethanol and 0.5 mL distilled water was added dropwise into solution A within 30 min. After this operation, the resulting mixture was hydrolyzed at room temperature for 1 h under stirring and then a transparent light yellow sol was obtained, following by ageing in air at room temperature for 24 h. Then, the sample was dried at 80 °C for 2 h. After cooling and grinding, the powder xerogel was obtained. The xerogel samples were calcined at 400 °C, 500 °C, 600 °C, 700 °C and 800 °C in a muffle furnace for 1 h, respectively. TiO_2 nanopowders with different phase composition and different crystallite size were produced. By the same method, the Fe^{3+} doped nano-sized TiO_2 was prepared by replacing solution B with a mixture containing 5 mL of absolute ethanol and 0.5 mL of 0.1 mol/L $Fe(NO_3)_3$ solution, aged at 80 °C for 1 h, and calcined at 500 °C for 1 h.

Using a chemical oxidation method PANI/TiO_2–Fe^{3+} nanocomposite was synthesized. A solution of $K_2S_2O_8$ (5 mmol) in a 50 mL of 0.1 mol/L HCl was mixed with double distillation aniline (ANI, 5 mmol) in a 50 mL of 0.1 mol/L HCl solution. Then, 0.5 g of TiO_2–Fe^{3+} nanoparticles obtained was added into the system. The mixture was left for polymerization for 2 h at 5 °C under stirring. After filtrating, the precipitate was washed with 0.1 mol/L HCl and distilled water, respectively. Then, the blackish green solid was dried at 60 °C for 2 h.

Characterization of products

The phase composition of the products was analyzed by X-ray powder diffraction (XRD), using a Japan Rigaku D/max-B X-ray diffraction meter with Cu$K\alpha$ radiation (λ = 1.5418 Å), tube current 40 mA and voltage 100 kV.

AFM and TEM technologies were used to examine the morphology and microstructure of the products. The AFM images of the products were obtained with a Seiko SPI 3800 scanning probe microscope in contact mode, using silicon nitride (Si_3N_4) cantilever and integral tips. The sample used for AFM observation was prepared by dispersing some products in absolute ethanol followed by the ultrasonic vibration for 30 min, placing a drop of dispersion onto a mica sheet, then calcining the mica substrate at 650 °C for 1.5 min in a muffle furnace. The TEM images were taken on a JEM-100SX apparatus with a 100 kV accelerating voltage. The sample powder was dispersed in absolute ethanol and cast on carbon-coated copper grid.

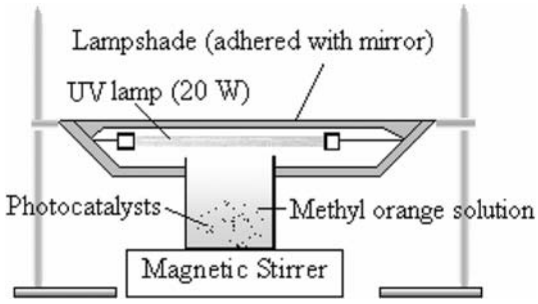

Fig. 1 Schematic diagram of photodegradation of methyl orange

IR spectra were recorded on a Thermo Nicolet 5700 FT-IR Spectrometer from 2000 cm^{-1} to 400 cm^{-1}. Sample was mixed with KBr powders and pressed into a pellet. Spectra were corrected for the moisture and carbon dioxide in the optical path.

Photocatalytic experimental

The photocatalytic activity of the products was evaluated by the photodegradation of methyl orange, using a 250 mL beaker, containing 100 mL of 20 mg/L methyl orange solution and 0.1 g photocatalysts. A UV lamp (20 W, λ = 253.7 nm) or sunlight was used as light source, respectively. In the process of UV irradiation, the distance between the surface of solution and the light source was 10 cm, as shown in Fig. 1.

At different time intervals during the irradiation, a 2 mL solution was picked out and centrifugalized for spectrophotometric detection. The absorbance A at 470 nm for methyl orange was measured in a 721B spectrophotometer, and the A value was used to estimate the photocatalytic degradation rate D of methyl orange according to the equation:

$$D = (A_0 - A_t)/A_0 \times 100\% \quad (1)$$

where A_0 is the initial absorbance of methyl orange, t is the reaction time and A_t is the absorbance at time t.

Results and discussion

The effect of calcination temperature on the phase composition of TiO_2 nanopowder

The XRD patterns of TiO_2 nanopowders heat-treated at different temperatures are shown in Fig. 2. It

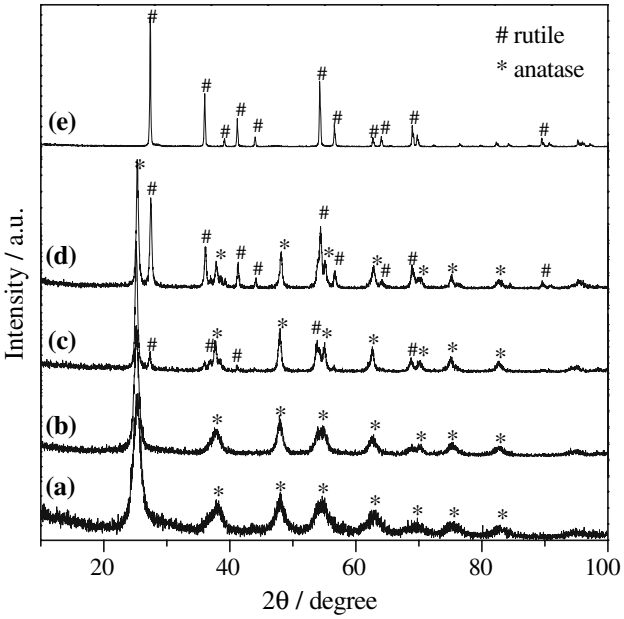

Fig. 2 The XRD patterns of the TiO_2 nanopowders obtained at different calcination temperature (**a**) 400 °C; (**b**) 500 °C; (**c**) 600 °C; (**d**) 700 °C; (**e**) 800 °C

indicated the formation of anatase TiO_2 at approximately 400 °C, which coincides well with the earlier report [9]. The crystallization temperature is relatively low but not the lowest. The sharp peak at 500 °C means the increase of crystallization degree. With the calcination temperature increasing, the peak number corresponding to the rutile phase increases. That is, the higher temperature is benefit to the formation of rutile nanopowder. Moreover, the pure rutile nanopowder was obtained at 800 °C.

The weight fractions of anatase to rutile in TiO_2 nanopowder were calculated by using the following equation [10]:

$$f_A = \frac{1}{1 + 1.26 I_R / I_A} \tag{2}$$

Fig. 3 Anatase content of TiO_2 nanopowders at different calcination temperature

where f_A is the weight fraction of anatase, I_R is the intensity of the (110) reflection of rutile, and I_A is the intensity of the (101) reflection of anatase. Figure 3 shows the anatase content in the TiO_2 nanopowders as a function of the calcination temperature.

It may be noticed that when the calcination temperature is below 700 °C, the diffraction peaks are relatively broad, particularly for the lower temperatures. The broadening peaks are caused by the small crystallite. The crystallite size of nano-TiO_2 particle was calculated from Debye–Scherrer equation [11]:

$$\beta = k\lambda / D \cos\theta \tag{3}$$

where λ is the X-ray wavelength, k is the shape factor, D is the average diameter of the crystals (in angstroms), θ is the Bragg angle (in degrees) and β is the line-width measured at half-height and expressed in unit of 2θ. The value of k depends on the Miller index of the reflecting planes and the shape of the crystals [12]. If the shape is unknown, k is often assigned as a value of 0.89. To analyze the X-Ray diffraction pattern of the TiO_2 nanopowders, we choose the reflection peaks at $2\theta = 25.3°$ for anatase and $2\theta = 27.4°$ for rutile to calculate the diameter of products. Thereby, the average diameters of the TiO_2 nanopowders obtained at different calcination temperature are 15 (a), 18 (b), 38 (c), 52 (d), and 87 nm (e), respectively. In the study of polymorph of TiO_2, the anatase was the most used phase for photocatalytic application [13]. Therefore, the anatase phase TiO_2 obtained at 500 °C was used to evaluate its photocatalytic activity in the further experiments.

XRD of PANI/TiO_2–Fe^{3+} nanocomposite

Figure 4 shows the XRD patterns of the TiO_2 nanopowder (a), TiO_2–Fe^{3+} nanopowder (b), and PANI/TiO_2–Fe^{3+} nanocomposite (c), respectively. Figure 4b

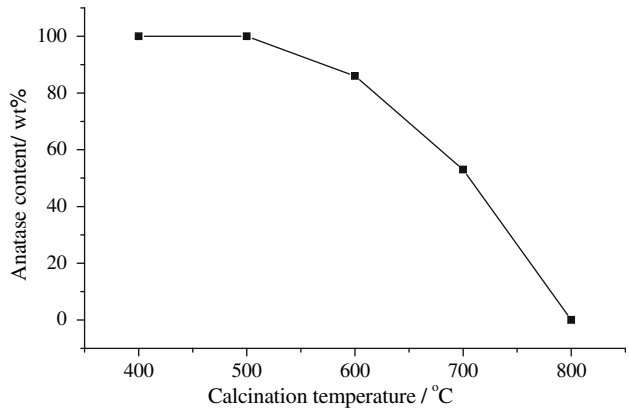

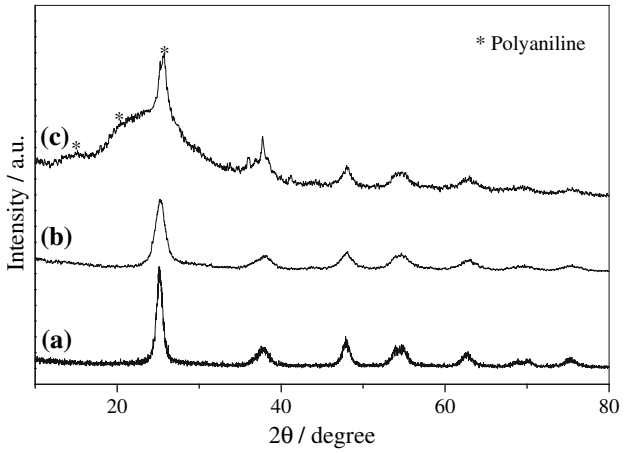

Fig. 4 The XRD patterns of the products: (**a**) TiO_2, (**b**) TiO_2–Fe^{3+}, (**c**) PANI/TiO_2–Fe^{3+} T = 500 °C, $[Fe^{3+}] = 1 \times 10^{-3}$ mol/L, $[PANI] = 5 \times 10^{-2}$ mol/L

indicates that Fe species well dissolved into the TiO_2 crystal because the peak corresponding to Fe compound did not appear in the X-ray diffraction pattern. The broadening of peak reflects that the doped Fe species inhibits the particle growth, which is benefit to the photocatalytic property of TiO_2. As shown in Fig. 4c, the XRD pattern of PANI/TiO_2–Fe^{3+} composite consists of the characteristic peaks of anatase phase TiO_2 and one broad peak locates at $2\theta = 15 \sim 30$. The positions of all peaks of TiO_2 are in agreement with the pure anatase TiO_2 because the PANI is polymerized after forming the nano-TiO_2 particles. In the broad peaks, the characteristic peaks (2θ = 14.9°, 19.9°) of PANI can be seen. The characteristic peak (2θ = 25.3°) of TiO_2 overwhelmed the characteristic peak (2θ = 25.4°) of PANI. Because the existing of the hydrogen bonding action between the hydroxyl groups on the surface of TiO_2 nanoparticles and the imine groups in the PANI molecular chains, we can deduce that the PANI in the composite deposits on the surface of TiO_2 nanoparticles. An IR study is necessary to confirm further whether the PANI is bonded with the TiO_2 nanoparticles or is just deposited on the surface of TiO_2. Corresponding results will be seen in "FT-IR spectral analysis" section. The average diameters of TiO_2, TiO_2–Fe^{3+} and PANI/TiO_2–Fe^{3+} are 18, 8 and 25 nm, respectively.

Morphology analysis

The AFM and TEM images of the products are shown in Figs. 5 and 6, respectively. Figures 5a and 6a indicate that TiO_2 nanoparticles are ball-like in shape with diameters of 20 nm and 15 nm, respectively. However, TEM image indicates that the TiO_2 nanoparticles are aggregated in aqueous solution. From Figs. 5b and 6b we can see that the diameter of TiO_2–Fe^{3+} nanoparticle is smaller than TiO_2 and the sizes are *ca* 12 nm and 10 nm, respectively. It means that the doped Fe species inhibits the growth of TiO_2 nanoparticle, which is consistent with the results of XRD. Figure 5c shows that a well dispersed, a narrow size spherical nanoparticle was obtained, and the grain size is about 25 nm. Figure 6c shows that the nanocomposite has a core-shell structure with TiO_2 as core and PANI as shell. The possible reason is that a part of aniline diffused into the HCl solution reacting with HCl to form aniline hydrochloride, causing the existence of the free aniline and aniline hydrochloride molecule on the surface of TiO_2–Fe^{3+} nanoparticle. The next reaction will generate PANI. A part of TiO_2–Fe^{3+} nanoparticle surface would be enshrouded with PANI, leading to the formation of core-shell structured PANI/TiO_2–Fe^{3+} nanocomposite.

FT-IR spectral analysis

Figure 7 shows the FT-IR spectra of TiO_2 nanopowder (a), TiO_2–Fe^{3+} nanopowder (b), and PANI/TiO_2–Fe^{3+} nanocomposite (c), respectively. Figure 7c indicates that the main characteristic peaks of PANI appear in the composite, which are assigned as follows: C=N and C=C stretching modes for the quinonoid and benzenoid units occur at 1563 cm^{-1} and 1484 cm^{-1}, the bands at 1296 cm^{-1} and 1225 cm^{-1} have been attributed to

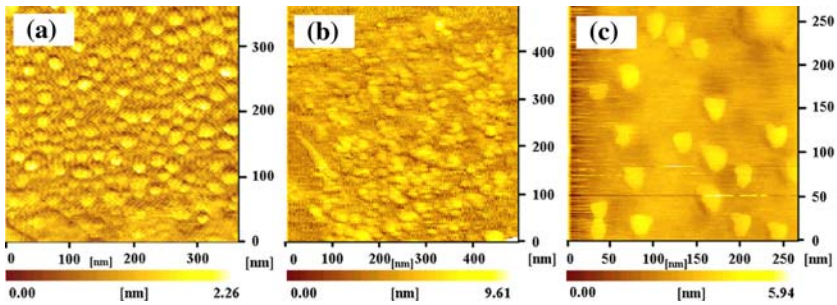

Fig. 5 The AFM images of the products: (**a**) TiO_2, (**b**) TiO_2–Fe^{3+}, (**c**) PANI/TiO_2–Fe^{3+} T = 500 °C, $[Fe^{3+}] = 1 \times 10^{-3}$ mol/L, $[PANI] = 5 \times 10^{-2}$ mol/L

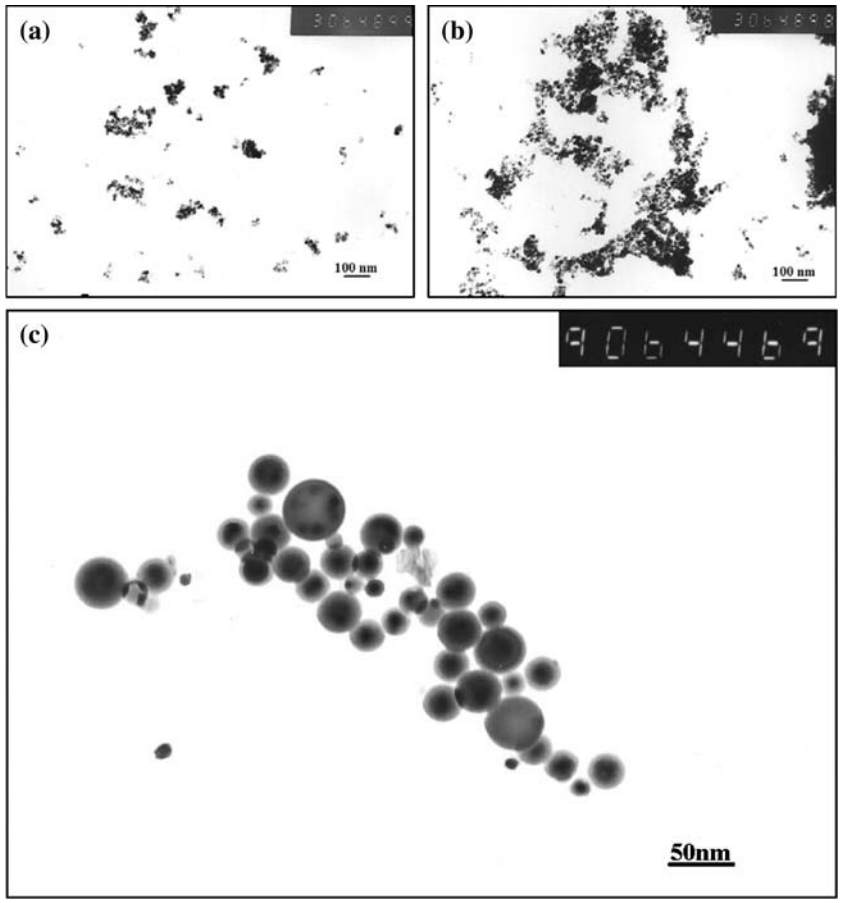

Fig. 6 The TEM photographs of the products: (**a**) TiO_2, (**b**) TiO_2–Fe^{3+}, (**c**) PANI/TiO_2–Fe^{3+} T = 500 °C, [Fe^{3+}]= 1×10^{-3} mol/L, [PANI] = 5×10^{-2} mol/L

C–N stretching mode for benzenoid unit, while the peak at 798 cm^{-1} is associated with C–C and C–H for benzenoid unit. Besides, Fig. 7c reveals that the maximum peak of TiO_2 (603 cm^{-1}) occurs in the composite. However, all bands shift slightly to the lower wavenumber compared with PANI doped with HCl [14] and pure TiO_2. In addition, two newpeaks (1373 cm^{-1} and 1018 cm^{-1}) have appeared in the PANI/TiO_2–Fe^{3+} nanocomposite. These results indicate that a strong interaction exists between the interface of PANI and nano-TiO_2. That is, when the $K_2S_2O_8$ is added to the reaction system, the polymerization proceeds on the surface of TiO_2 nanoparticle. It leads to adhesion of PANI to the TiO_2 nanoparticles. Because the titanium is a transition metal and titanic has an intense tendency to form coordination compound with nitrogen atom in PANI molecular, such adhesion will not only constrain the motion of PANI chains, but also restrict the modes of vibration in PANI molecule. Finally, the strong interaction causes the shifts of bands and the appearance of new peaks. Moreover, hydrogen bond between the hydroxyl groups on the surface of TiO_2–Fe^{3+} nanoparticle and the imine group in the PANI molecular chain is also contributory to the shift of bands. To sum up, FT-IR measurements show that PANI and TiO_2 nanoparticles are not simply blended or mixed up, but a strong interaction exists at the interface of nano-TiO_2 and PANI.

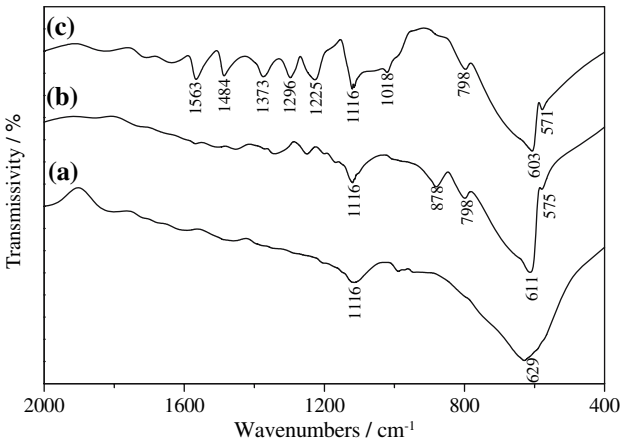

Fig. 7 FT-IR spectra of the products: (**a**) TiO_2, (**b**) TiO_2–Fe^{3+}, (**c**) PANI/TiO_2–Fe^{3+} T = 500 °C, [Fe^{3+}] = 1×10^{-3} mol/L, [PANI] = 5×10^{-2} mol/L

Photocatalytic activities

The degradation efficiency of methyl orange is shown in Fig. 8. It can be seen that within 60 min, only 27.2 % and 67.2 % of methyl orange were degraded by sunlight and UV irradiation in the presence of alone nano-TiO_2, respectively. If using TiO_2–Fe^{3+} as photocatalyst, the degradation efficiency reaches up to 32.2% and 77.7%, respectively, in the same conditions. It is noteworthy that the degradation efficiency reaches 80.8% and 95.2% after 10 min and 30 min by using PANI/TiO_2–Fe^{3+} as photocatalyst under the irradiation of UV light, while the degradation efficiency of 35.2% and 70.3% was obtained under sunlight. This suggests that PANI plays a very important role in the photocatalytic reaction. Since Degussa P-25 Nano-TiO_2 (P25) is considered as an excellent photocatalyst, the photocatalytic behavior of P25 was also measured as a reference to compare with that of the prepared catalysts. The results indicate that there is a similar activity between the P25 and the proposed TiO_2. A conclusion may be drawn that the coating TiO_2–Fe^{3+} with PANI can enhance remarkably the photocatalytic activities of TiO_2 and result in the shift towards visible side.

The photocatalytic degradation of methyl orange is a pseudo-first-order reaction [15] and its kinetics may also be expressed as the following equation [16]:

$$\ln(A_0/A_t) = kt \tag{4}$$

where k is the apparent rate constant and a linear regression program can be employed to calculate it. In this study, the value of k is 5.64×10^{-2}, which is even higher than that of P25 $(k = 4.19 \times 10^{-3})$ [17].

Mechanism of the promoted photocatalysis

The heterogeneous photocatalysis degradation of methyl orange by semiconductors has been widely investigated and the photocatalytic mechanism of TiO_2 and Fe^{3+} doped TiO_2 photocatalysts have been reported [18, 19]. As a conducting polymer, previous experimental and theoretical works have shown that PANI has semiconductor capability and large band gap [20]. This is similar to TiO_2 semiconductor. When TiO_2 was coated with PANI, the interface between the two phases may act as a rapid separation site for the photogenerated electrons and holes due to the difference in the energy level of their conduction bands (CB) and valence bands (VB). Figure 9 illustrates the photoexcitation and the process of charge separation in PANI/TiO_2–Fe^{3+} photocatalyst system. It indicates that when PANI/TiO_2–Fe^{3+} was irradiated with UV light, electrons in valence bands of PANI and TiO_2 can be excited to their conduction bands and left holes at their surface. Because the conduction band of PANI is higher than that of TiO_2, electrons in the conduction band of PANI are easily moved into the conduction band of TiO_2, and then the holes in the PANI are filled with the redox couples, which is advantageous for the efficient charge carrier separation. Moreover, TiO_2 was coated with PANI partly, both TiO_2 and PANI can contact the solution directly. The photogenerated holes in the PANI species can transfer up to the interface between PANI species with the solution. Thus, the photogenerated holes in the TiO_2 particles can transfer up to the interface between TiO_2 particles with solution and/or penetrate the PANI species; and then arrive up to the interface between PANI species with the solution. Due to their strong oxidation ability, these photogenerated holes may react directly with the surface-sorbed organic molecules to form $R^{+}\cdot$ or ·OH radicals. In the case, the methyl orange molecules are attacked by hydroxyl radicals and generate organic radicals or other intermediates. Finally, the parent compounds and intermediates are oxidized into CO_2, SO_2, HNO_3 and H_2O.

Therefore, surface sensitization of TiO_2 with PANI will be beneficial to decreasing the electron and hole

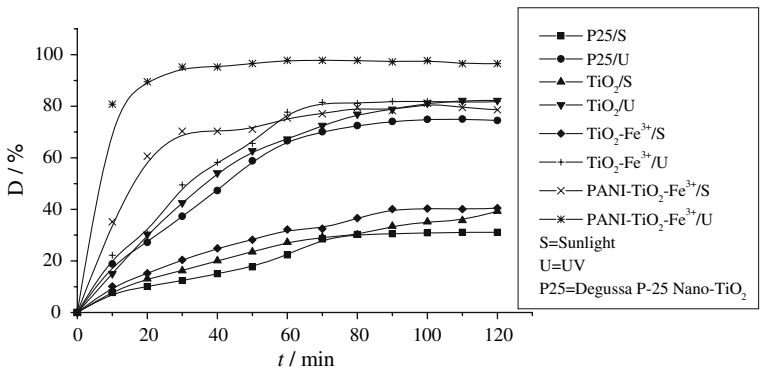

Fig. 8 The results of photodegradation for methyl orange solution (20 mg/L) in different conditions [catalyst] = 1 g/L

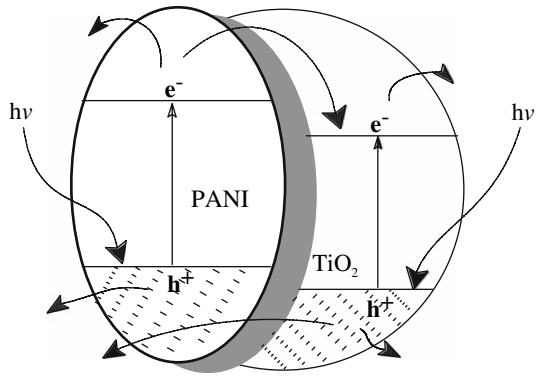

Fig. 9 Photoexcitation and the charge separation in PANI/TiO_2–Fe^{3+} photocatalyst

recombination rate, increasing the quantum yield of the photocatalytic process and promoting the photocatalytic activity of TiO_2.

Conclusion

In summary, PANI/TiO_2–Fe^{3+} nanocomposite exhibits higher photocatalytic activity than pure anatase TiO_2, Fe-doped TiO_2 nanopowder, as well as P25 photocatalyst. The excellent property has been evaluated by the degradation of methyl orange under the UV irradiation. Meanwhile, TiO_2 modified by PANI can widen the visible optical absorption region and increase obviously the photocatalytic activity in the visible region. The different conduction band, valence band and forbiddenzone width of TiO_2, PANI overlapped and the separate rate of charges in the composite was enhanced. The proposed method may be used for the synthesis of the nanocomposite of PANI with various inorganic nanoparticles.

Acknowledgements This work was supported in part by the Combined Project between the Educational Commission and the Economic Commission of Gansu Province (99CX-04, 0310B-08), the Natural Science Foundation of Gansu Province (3ZS041-A25–028), EYTP of MOE. China, and the Invention Project of Science & Technology (KJCXGC-01, NWNU), China.

References

1. Fujishima A, Honda K (1972) Nature 37:238
2. Guo XJ, Yuan L, Qi YL, Li XE, Yang W, Gao JZ (2004) Rare Metals 23:352
3. Xu ZL, Yang QJ, Xie C, Yan WJ, Du YG, Gao ZM, Zhang JH (2005) J Mater Sci 40:1539, DOI: 10.1007/s10853-005-0599-6
4. Yu JG (2004) Rare Metals 23:289
5. Yan XL, He J, Evans DG, Duan X, Zhu YX (2005) Appl Catal B Environ 55:243
6. Khanna PK, Lonkar SP, Subbarao VVVS, JUN KW (2004) Mater Chem Phys 87:49
7. Alan GM, Arthur JE (1995) Synth Met 69:85
8. Somani PR, Marimuthu R, Mulik UP, Sainkar SR, Amalnerkar DP (1999) Synth Met 106:45
9. Arroyo R, Córdoba G, Padilla J, Lara VH (2002) Mater Lett 54:397
10. Spurr RA, Myers H (1957) Anal Chem 29:760
11. Langford JA, Wilson AJC (1978) J Appl Crystallogr 11:102
12. Klong HP, Alexander LE (1954) In: X-ray diffraction procedures for crystalline and amorphous solids. Wiley, New York, p 491
13. Sclafani A, Herrman JM (1996) J Phys Chem 100:13655
14. Li XW, Chen W, Bian CQ, He JB, Xu N, Xue G (2003) Appl Surf Sci 217:16
15. Yu JG, Zhao XJ (2000) J Catal 21:213 (in Chinese)
16. Sonawane RS, Kale BB, Dongare MK (2004) Mater Chem Phys 85:52
17. Piscopo A, Robert D, Weber JV (2001) J Photochem Photobiol A Chem 139:253
18. Linsebigler AL, Lu GQ, Yates JT (1995) Chem Rev 95:735
19. Měšťánková H, Mailhot G, Jirkovský J, Krýsa J, Bolte M (2005) Appl Catal B Environ 57:257
20. Vaschetto ME, Monkman AP, Springborg M (1999) J Mol Struct (Theochem) 468:181